Incommensurate Modulation in the Microporous Silica SSZ-24

Zheng Liu,[a, f] Nobuhisa Fujita,[a, g] Osamu Terasaki,*[a, b] Tetsu Ohsuna,[c] Kenji Hiraga,[c] Miguel A. Camblor,[d] Maria-José Díaz-Cabañas,[d] and Anthony K. Cheetham[e]

Abstract: A detailed investigation of the structure of microporous silica, SSZ-24, is presented. It is shown by X-ray powder diffraction and ^{29}Si MAS NMR experiments that the structure deviates from the previously proposed $AlPO_4$-5-type structure. At room temperature, electron diffraction (ED) patterns exhibit extra diffraction spots, which can be attributed to an incommensurate structural modulation along the *c* axis. This in turn results in a pleat pattern in real space with two different intervals arranged aperiodically along the *c* axis, as observed with high-resolution electron microscopy (HREM). The modulated structure may easily turn into a disordered one through excessive electron irradiation or heat-treatment. In order to understand the origin of the modulation, soft phonon-modes of the ideal premodulated structure were analyzed by the use of the rigid-unit-mode model. The distribution of soft modes in reciprocal space might correspond roughly to diffuse streaks that could be observed in the diffraction patterns at higher temperatures. It was found that several phonon branches soften at specific wave vectors, which are incommensurate with respect to the original period and might be responsible for the modulation. We present a simple analytic treatment to deduce the wave vectors and associated displacement eigenvectors for the incommensurate soft-modes.

Keywords: electron microscopy · rigid-unit-mode model · silicates · soft phonon-modes · zeolites

Introduction

The microporous material SSZ-24, the silica analogue of the zeolite $AlPO_4$-5 (AFI), forms a hexagonal silica framework without cations inside large uniaxial channels along the *c* direction. The space group of $AlPO_4$-5 reported formerly was *P*6*cc*[1, 2] and higher symmetry *P*6/*mcc*.[3] The average structure of SSZ-24 has been analyzed previously by synchrotron powder X-ray diffraction (XRD), and the space group was determined to be *P*6/*mcc*.[4] However, the structure is still somewhat controversial, because if one assumes the space group to be rigorously fulfilled, several Si-O-Si angles in the unit cell must be close to 180°; this is unlikely to occur in reality. The problem was overcome in the original powder XRD refinement by displacing the O atom concerned from its high symmetry position and lowering its occupancy factor. The angles can also be dropped to 140–150° by reducing the symmetry to *Pcc*2 (orthorhombic)[5] or *P*6 (hexagonal).[6] In the case of the aluminophosphate $AlPO_4$-5, there are also linear angles in the initially assigned *P*6*cc* symmetry that can be eliminated by lowering the symmetry to *P*6. Synchrotron XRD data of $AlPO_4$-5 shows that the symmetry must be even lower (possibly *Pcc*2).[7]

Accurate knowledge of the structure of zeolites is of significant fundamental and applied importance in zeolite science. From XRD and ^{29}Si MAS NMR data of calcined SSZ-24 samples prepared by four different methods in our own laboratory, we realized that the structure of this material must be much more complex than reported. This prompted us to study SSZ-24 by HREM and ED, which revealed a modulation of the structure in the *c* direction.

In order to understand the origin of the modulation, we used the rigid-unit-mode model,[8, 9] that is, a coarse-grained

[a] Prof. O. Terasaki, Dr. Z. Liu, Dr. N. Fujita
CREST, JST, Department of Physics, Graduate School of Science
Tohoku University, Sendai 980-8578 (Japan)
Fax: (+81) 22-217-6475
E-mail: terasaki@msp.phys.tohoku.ac.jp

[b] Prof. O. Terasaki
Center of Interdisciplinary Research, Tohoku University
Sendai 980-8578 (Japan)

[c] Dr. T. Ohsuna, Prof. K. Hiraga
Institute for Materials Research, Tohoku University
Sendai 980-8577 (Japan)

[d] Dr. M. A. Camblor, Dr. M.-J. Díaz-Cabañas
Industrias Químicas del Ebro, Polígono de Malpica
Calle D, no 97 50057 Zaragoza (Spain)

[e] Prof. A. K. Cheetham
Materials Research Laboratory, University of California
Santa Barbara CA 93106 (USA)

[f] Dr. Z. Liu
Present address:
Institute of Multidisciplinary Research for Advanced Materials
Tohoku University, Sendai 980-8577 (Japan)

[g] Dr. N. Fujita
Present address: Research Institute of Electrical Communication
Tohoku University, Sendai 980-8577, Japan

  0947-6539/02/0819-4549 $ 20.00+.50/0

model with the following important features of framework materials. Framework materials such as silicates and zeolites consist of basic tetrahedral units, TO_4 (T = Si or Al), in which each oxygen atom is shared by two neighboring units. The basic units are very rigid because of the large energies required to stretch/shorten the T–O bond and to change the relative angles of the four T–O bonds from the most stable tetrahedral configuration. On the other hand, the change of relative configurations of neighboring units, through a bending or a rotation with respect to their shared O atom, requires less energy. It is known that these materials undergo various structural phase transitions that cause displacement at temperatures below 1000 K. The relevant deformations involve little change in shape of the individual TO_4 units, that is, the integrity of the tetrahedral shape is almost retained. The possibility of such flexible deformations manifests itself in the existence of soft modes of vibration in higher-temperature phases. In the context of zeolites, the rigid-unit-mode model has been extensively used to analyze the framework flexibilities, which are of substantial importance in understanding the phase transitions that cause displacement as well as the adsorption characteristics of cations in these materials.[10, 11]

Experimental Section

Pure silica SSZ-24 was synthesized by four different methods, depending on the organic structure direct agent (SDA) cation (*N*-methylsparteinium (MSPT) or *N*,*N*,*N*-trimethyladamantammonium (TMAda)) and on the mineralizer (hydroxide or fluoride). Thus, the synthesis methods and the materials obtained will be denoted as MSPT–F, MSPT–OH, TMAda–F and TMAda–OH.

SDA syntheses: *N*-methylsparteinium was synthesized from a solution of (−)-sparteine in acetone, to which CH_3I was added slowly and under stirring. After 24 hours, diethyl ether was added, and the mixture was filtered. The obtained solid was recrystallized in methanol/ethyl acetate and was shown by chemical analysis and ^1H and ^{13}C NMR in $CDCl_3$ to be *N*-methylsparteinium iodide.

N,*N*,*N*-trimethyl-L-adamantammonium was synthesized by slowly adding CH_3I to an ice-cooled solution of L-adamantamine in $CHCl_3$, in the presence of $K_2CO_3 \cdot 1.5H_2O$. After 7 days at RT, the mixture was filtered, and the solid was washed with $CHCl_3$. The clear solution was then mildly heated under vacuum to evaporate the solvent, and the obtained solid was washed with diethyl ether and dried under vacuum. Chemical analysis and ^1H and ^{13}C NMR in $CDCl_3$ showed the product to be *N*,*N*,*N*-trimethyl-L-adamantammonium iodide.

Prior to the zeolite syntheses, both iodide salts were exchanged to their hydroxide forms by anion exchange in aqueous solution by using an anion resin (Dowex-1).

Zeolite syntheses

MSPT–OH method: An aqueous solution of MSPTOH (29.22 g, 0.82 mol OH per kg) was mixed with a solution of KOH (0.34 g) in water (44.08 g) and with Aerosil 200 (7.20 g). The mixture was stirred for 1 hour. After being heated at 150 °C for 21 days, the mixture was filtered, and the solid was washed with distilled water and dried at 100 °C. The yield of SSZ-24 was 9.63 g per 100 g gel. The composition of the starting mixture was SiO_2/MSPTOH/KOH/H_2O = 1:0.20:0.05:31.

MSPT-F method: Tetraethylorthosilicate (20.80 g) was hydrolyzed in an aqueous solution of MSPTOH (31.84 g, 1.57 mol OH per kg). The mixture was left stirring for complete evaporation of the ethanol produced in the hydrolysis and the water needed to achieve the desired final composition. Then, an aqueous solution of HF (2.08 g, 48 %) was added, and the mixture was thoroughly homogenized by hand. After 7 days at 175 °C, the mixture was filtered, and the solid was washed with distilled water and dried at 100 °C. The yield of SSZ-24 was 19.23 g per 100 g gel. The composition of the starting mixture was SiO_2/MSPTOH/HF/H_2O = 1:0.50:0.5:7.5.

TMAdaOH method: This method is described in ref. [12] KOH (0.16 g) was dissolved in water (6.32 g), then a solution of TMAdaOH (5.79 g, 0.525 mol OH per kg) and Aerosil 200 (1.22 g(were added. The mixture was stirred for 2 h. After 6 days at 150 °C, the mixture was filtered, and the solid was washed with distilled water. The yield of SSZ-24 was 6.52 g per 100 g gel. The composition of the starting mixture was SiO_2/TMAdaOH/KOH/H_2O = 1:0.15:0.12:44.

TMAda-F method: A mixture of starting nominal composition SiO_2/TMAdaOH/HF/H_2O 1:0.50:0.50:20 was heated for 12 days at 150 °C. The synthesis was intended to crystallize SSZ-23 (see ref. [13] where further synthesis details can be also found). However, the final pH of the mother liquor was too high (11.1 rather than < 9), and the product was pure SSZ-24.

Characterization: Phase purity of the materials was determined by conventional powder X-ray diffraction (XRD) by using a Philips X'Pert diffractometer. C, H, and N contents were determined with a Carlo Erba 1106 elemental analyzer. The fluoride content was determined by using an ion-selective electrode connected to a Mettler Toledo 355 ion analyzer after dissolution of the as-made solids by a standard procedure.[14] Thermogravimetric analyses were performed on a NETZSCH STA 409 EP thermal analyzer in the 293 – 1073 K range with about 0.0200 g of sample, a heating rate of 10 K min^{-1}, and an air flow of 6 L h^{-1}. The ^{29}Si MAS NMR spectra of the solids were recorded on a Varian VXR 400 SWB spectrometer at a spinning rate of 5.5 kHz at a ^{29}Si frequency of 79.459 MHz, with a 55.4° pulse length of 4.0 μs, and a recycle delay of 60 s.

Finally, crystal size and morphology were monitored by scanning electron microscopy (SEM) on a JEOL JSM-6300 microscope.

For TEM measurements, the sample was first crushed by mortar, then dispersed in ethanol (99.9 vol. %) by ultrasonic method, and finally, dropped onto a carbon microgrid. High-resolution electron microscopy (HREM) observations were performed with a 400kV electron microscope (JEM-4000EX) at room temperature. High temperature observations were carried out by 1250 kV EM (JEM-1250) with a top-entry high temperature stage.

Results and Discussion

Pure silica SSZ-24 was crystallized by using two different SDAs and two different mineralizers. The chemical compositions of the four types of as-made samples are listed in Table 1. Among the four as-made samples, it is clear that only MSPT-F-SSZ-24 may be essentially free of connectivity defects, since only in that sample may the concentration of organic cations be fully balanced by fluoride anions. Nevertheless, the concentration of silanol groups in all the calcined samples is rather low (see ^{29}Si MAS NMR results below); this indicates significant annealing of defects upon calcination.

X-ray diffraction: All the samples were identified as SSZ-24. The powder X-ray diffractograms of the calcined samples are shown in Figure 1. The SSZ-24 samples prepared from MSPT contained a very small amount of impurities. More impor-

Table 1. Chemical composition of the as-made SSZ-24 samples.

Synthesis	g in 100g of zeolite						mol [u.c.]	
Method	N	C	H	F	SiO_2 %[a]	C/N[b]	SDA	F
TMAdaOH	0.71	7.98	1.49	–	88.68	13.2	0.82	–
TMAda-F	0.87	9.00	1.52	0.31	88.38	12.1	1.01	0.27
MSPT–OH	1.32	9.20	1.52	–	86.33	8.1	0.79	–
MSPT-F	1.36	9.55	1.45	0.92	86.93	8.2	0.80	0.80

[a] Residue after the thermogravimetric analysis. [b] The C/N mol ratios in TMAda and MSPT are 13 and 8, respectively.

0947-6539/02/0819-4550 $ 20.00+.50/0 *Chem. Eur. J.* **2002**, *8*, No. 19

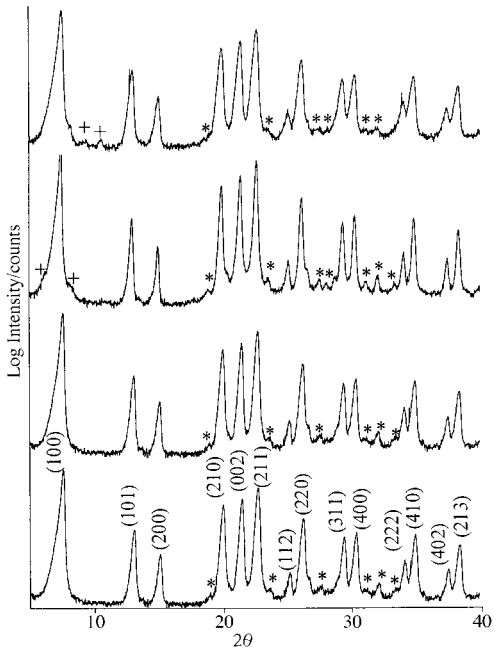

Figure 1. Powder XRD profile of SSZ-24. $Cu_{K\alpha}$ radiation. From the top, the profiles of TMAdaF, TMAdaOH, MSPT-OH, and MSPT-F.

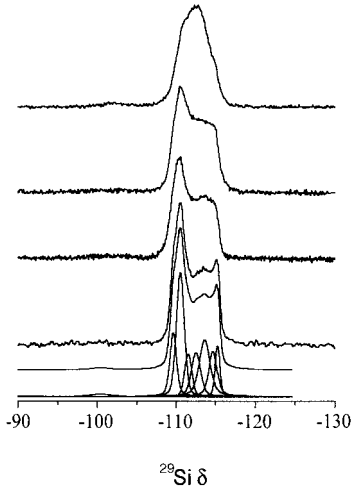

Figure 2. ^{29}Si MAS NMR spectrum of SSZ-24. From the top, the profiles of TMAdaF, TMAdaOH, MSPT-OH, and MSPT-F.

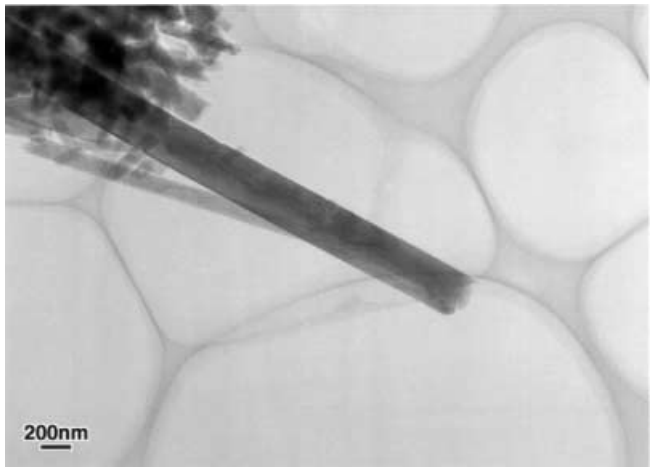

Figure 3. Low magnification TEM image of SSZ-24.

tantly, the four calcined samples showed very small reflections (marked with an asterisk in Figure 1) that could not be indexed by assuming hexagonal symmetry. The fact that these reflections appeared in the four samples with similar intensity, irrespective of the SDA or mineralizer, suggested that they may not correspond to an impurity phase. Furthermore, a careful inspection of the Rietveld plots of SSZ-24 in ref. [4] reveals small disagreements between the experimental and simulated profiles in the 25–35° 2θ region, in which we also find most of the peaks that cannot be indexed as hexagonal. This, together with the broadness and considerable asymmetry (apparent also at high reflection angles, and thus not due to axial divergence) of all the XRD reflections in Figure 1 suggests that the structure of calcined SSZ-24 may be more complex than the ideal one.

^{29}Si MAS NMR: In the reported *P*6/*mcc* space-group symmetry, SSZ-24 contains a single crystallographic site, so a single Q_4 resonance would be expected in the ^{29}Si MAS NMR spectrum. By contrast, Figure 2 shows a broad signal in the Q_4 region for all the samples. This signal is clearly composed of overlapping resonances, which are best resolved in the material prepared by the MSPT-F method. Attempts to deconvolute the spectrum of that sample required no less than 6 Gaussian–Lorentzian peaks in the Q_4 region. In all the spectra, there are indications of at least three overlapping resonances; this is strong evidence for a more complex structure.

TEM study: TEM was used in order to unravel the real structure of SSZ-24 (MSPT-F). SSZ-24 crystals have a long pillar shape with the uniaxial channel parallel to the long axis, which is known to be the *c* direction, as shown in Figure 3. Two HREM images with diffraction patterns taken from [001], which shows the uniaxial channel of SSZ-24, and [10 – 1] directions are shown in Figures 4 and 5, respectively. Corresponding ED patterns are inserted in the images. No extra reflections were observed for these incident directions. Simulated images based on the space group *P*6*cc* were also inserted together with framework models. The inserted simulated HREM images in Figures 4 and 5 fit very well with the experimental ones; this suggests that the structure of SSZ-24 should be discussed in terms of a modulation with a wave vector not observed in these incidences away from an AFI average structure.

However, diffraction patterns along the [010] and [1 – 10] directions show the appearance of forbidden parent reflections at *h*0*l* (*l* = odd) and *hhl* (*l* = odd) respectively, as shown by the arrows in Figure 6a and b. Note that such reflections as 001 and 111 etc. did not appear in the powder X-ray results; this illustrates that the sensitivity of X-ray experiments is low. Hence, it follows that the space group of the average structure of SSZ-24 cannot be *P*6/*mcc*, *P*6*cc*, or *Pcc*2, which were

  0947-6539/02/0819-4551 $ 20.00+.50/0

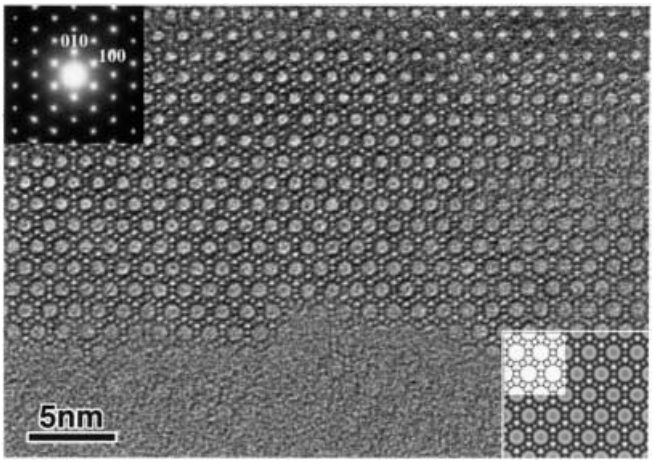

Figure 4. High resolution TEM image of SSZ-24 taken with [001] incidence.

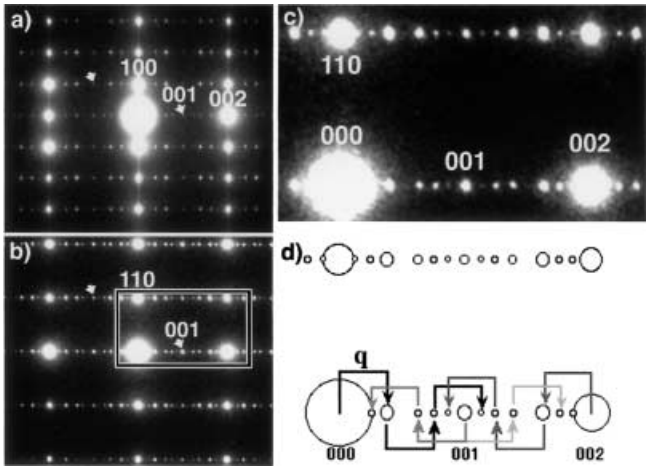

Figure 6. Electron diffraction patterns of SSZ-24 taken with a) [010] and b) [1 – 10] incidences, c) an enlarglar part of (b), and d) the corresponding schematic drawing.

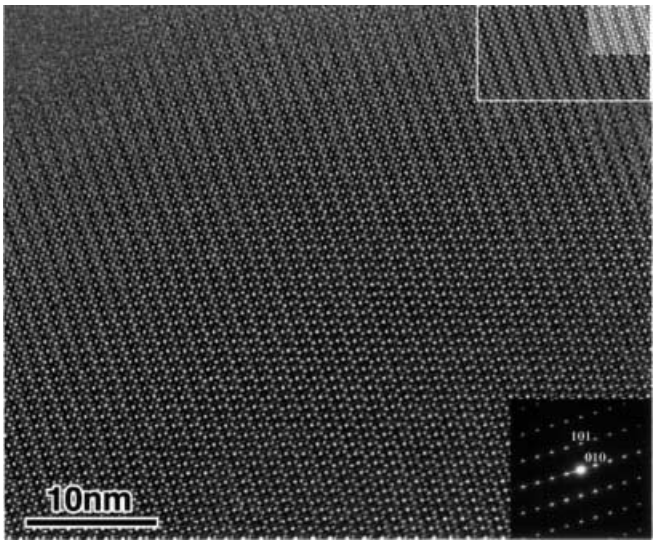

Figure 5. High resolution TEM image of SSZ-24 taken with [10 – 1] incidence.

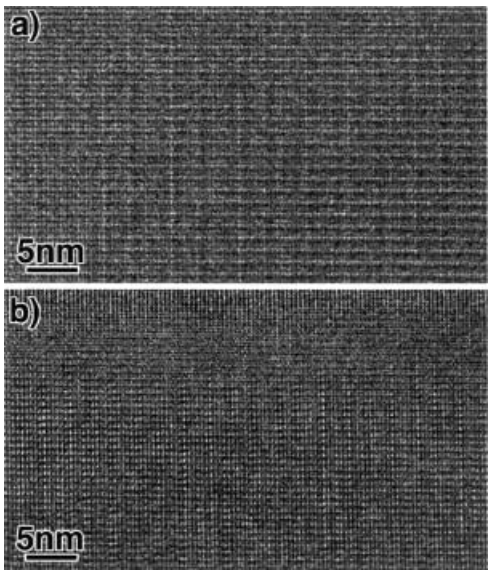

Figure 7. High resolution TEM image of SSZ-24 taken with a) [010] and b) [1 – 10] incidences.

mentioned earlier, since for these space groups the parent reflections with odd *l* would be extinct because of the *c* glides. Alternatively, a maximal nonisomorphic subgroup of *P*6/*mcc* (namely *P*622 or *P*6/*m*) or of *P*6*cc* (namely *P*6) could be a possible candidate.

It is also most important to note that the appearance of distinct satellite spots lying on the *c** axis, as in Figure 6a and b, shows that there are incommensurate modulations along the *c* direction. A detailed inspection of these incommensurate spots reveals that only one primary modulation wavevector ***q*** exists, and that the other spots are explained by higher-order harmonics thereof, so 4D crystallography might be a suitable approach for further quantitative analysis. This situation is shown in Figure 6c and d, where the common periodicity ***q*** is about 0.38 times that of the reciprocal lattice vector *c** . Correspondingly, one finds super-period structures (which have a brighter contrast of the lattice fringe) from the corresponding HREM images, shown in Figure 7a and b.

As found from in situ observation of the heat treatment by using heat staging in TEM, the distinct incommensurate satellite spots change to obscure diffuse lines at 100 °C, as shown in Figure 8; this illustrates that the incommensurate modulations change to disordered structure during the heat treatment These diffuse lines did not return to the former distinct incommensurate spots, even when the temperature was dropped down to 25 °C; this demonstrates that the change is irreversible. Electron beams always cause breaking of bonds in the framework, and even a small number of the induced defects might block reversible structural change with temperature.

Rigid-unit-mode model: As we have discussed so far, the structure of SSZ-24 is fairly well characterized by the space group *P*6/*mcc* up to a certain degree of resolution, but for finer resolutions the lowering of symmetry in the average structure as well as an incommensurate modulation is

0947-6539/02/0819-4552 $ 20.00+.50/0 *Chem. Eur. J.* **2002**, *8*, No. 19

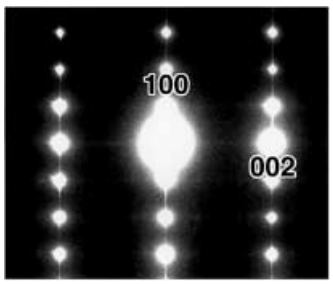

Figure 8. Electron diffraction patten of SSZ-24 at 100 °C.

observed at room temperature. These delicate features may have occurred through a phase transition that causes displacement, and are dominated by structural instability in the *higher temperature phase* with space group *P*6/*mcc*.

Let us take a simple model approach called the *rigid-unit-mode* (RUM) model, which was originally employed to investigate displacement-causing structural phase transitions in minerals.[8, 9] By the use of the structural data of Bialek et al,[4] we can model the structure of SSZ-24 as a network of tetrahedra interconnected by sharing their vertices, in which each tetrahedron is identified with SiO_4. The model is further optimized such that all the tetrahedral units are identical and exactly regular, while the space group and periodicity are retained. This leads to an idealized model of SSZ-24 in the higher-temperature phase (Figure 9a and b). The linkage of

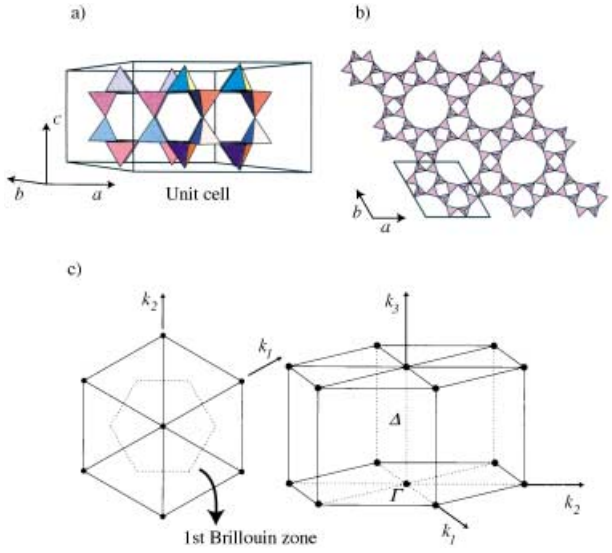

Figure 9. The optimized structure of SSZ-24. A 3D view of the primitive cell (a) as well as a single layer viewed along the *c* direction (b) are shown. Each tetrahedron represents a SiO_4 unit. c) The Brillouin zone for the hexagonal structure with symmetry points and axes labeled.

two connected units is assumed to behave like a hinge around which the two units can tilt or rotate freely with respect to each other. The finite rigidity of SiO_4 in reality is taken into account with the so-called *split-atom method*, which allows two vertices at one hinge to separate and assumes a potential energy between the two vertices. The potential energy is taken to be a harmonic one, $U(r) = kr^2/2$, with r being the distance between the vertices and k being the effective elasticity constant, which is assumed to be uniform.

As is mentioned earlier, a structural distortion involving little deformations of individual SiO_4 units costs little energy and leads to very small restoring forces. Hence relevant phonon modes would have very small frequencies; they are called *soft modes*. With the RUM approach, we can numerically analyze phonon frequency spectra for various framework structures and enumerate possible soft modes. As a result of initial optimization of the structure, one often finds a set of soft modes whose frequencies are exactly zero; these modes are called RUM. This makes it particularly appropriate to employ the RUM model for a detailed theoretical analysis of structural instabilities of a framework structure.

The phonon dispersion curves along the Δ line $(0,0,\alpha)$ of the reciprocal space (Figure 9c) can be calculated numerically (Figure 10). A quadruple set of RUM branches exists with

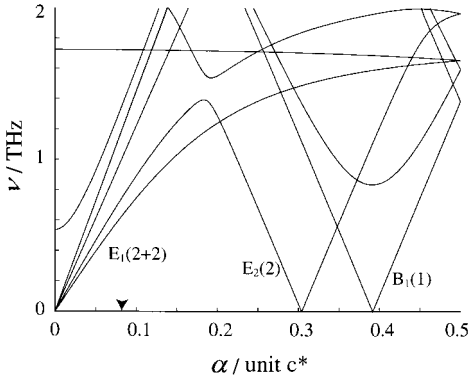

Figure 10. The lowest part of the phonon spectrum, $\tilde{\nu}(\mathbf{k})$, of the RUM model of SSZ-24 along the Δ line: $\mathbf{k} = (0,0,\alpha)$. Hidden along the horizontal axis are four RUM branches. At the Γ point, there are seven RUMs in addition to the three translational modes for acoustic branches. We have also RUMs at seemingly incommensurate wave vectors near $\alpha = 0.304$ and 0.392.

phonon frequency of exactly zero. There are also several isolated RUMs at the Γ point as well as at fractional wave vectors $\alpha = 0.304$ and 0.392, which are estimated at up to three digits of accuracy, accompanied by sharp drops of phonon branches. Note that some of the RUMs at the Γ point are thought to be responsible for the lowering of the symmetry of the average structure, that is, the reduction of *c* glides. Meanwhile, the fractional RUMs may be responsible for the modulation because they have *nontrivial* wave vectors that are incommensurate with the original periodicity.

As all the soft modes indicate possible flexible distortions of the idealized structure, their distribution in the reciprocal space was calculated. The distribution of soft modes whose frequencies are smaller than 0.01 THz in the ΓMLA-plane (α, 0, β) is shown with shadow in Figure 11, where black dots present the positions for fundamental reflections. Such analysis may correspond to the diffuse streaks that are observed in ED patterns for the higher-temperature phase. One can see that soft modes concentrate along the Δ line, especially at the three isolated points mentioned earlier, and also on the plane perpendicular to the c*(k_3) axis through the

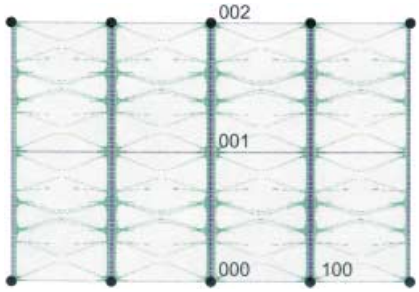

Figure 11. The distribution of the soft phonon modes in the ΓMLA-plane is shown. The shadowed points have at least one phonon mode with a frequency of less than 0.01 THz.

origin (Γ point). The following argument will be confined to phonon modes along the Δ line.

Symmetries of the RUMs: Although the intense accumulation of soft modes along the Δ line can cause a static disorder along the c direction when the temperature is lowered, experiment shows that there is only a single soft mode (or at most a few of them) responsible for the modulation. The mode should lie close to the observed wave vector $\alpha = 0.38$. The reason for nature's selecting this particular wave vector is a subtle question, and we have not been successful in providing a sufficient account for this. But it is worth noting that the wave vector is quite close to $\alpha = 0.392$, at which an isolated RUM is located. In the following, we present a simple argument based on the symmetries of the isolated RUMs that leads to analytic expressions for the relevant wave vectors and the associated lattice deformations.

We show the character table for the proper point group $G_{\mathbf{k}}$ of a wave vector $\mathbf{k} = (0,0,\alpha)$ in Table 2; note that $G_{\mathbf{k}}$ is isomorphic to the point group C_{6v}. Then each of the phonon branches along the Δ line has a symmetry property that is

Table 2. Character table for the point group C_{6v}.

IR	E	$2C_6$	$2C_3$	C_2	$3\sigma_v$	$3\sigma_d$
A_1	1	1	1	1	1	1
A_2	1	1	1	1	−1	−1
B_1	1	−1	1	−1	1	−1
B_2	1	−1	1	−1	−1	1
E_1	2	1	−1	−2	0	0
E_2	2	−1	−1	2	0	0

represented by an irreducible representation of $G_{\mathbf{k}}$. There are six types of irreducible representations, A_1, A_2, B_1, B_2, E_1, and E_2 as represented by the Mulliken symbols (see Table 2). The number of phonon modes for each wave vector coincides with the number of degrees of freedom per unit cell, which is $6 \times 24 = 144$ in our case. It is found that the 144 phonon branches are labeled as $12(A_1) + 12(A_2) + 12(B_1) + 12(B_2) + 48(E_1) + 48(E_2)$. The quadruple RUM branches along the horizontal axis in Figure 10 are found to have symmetry label E_1, while the RUMs at $\alpha = 0.304$ and 0.392 have the labels E_2 and B_1, respectively. Note that the irreducible representation E_2 is two-dimensional, so that the relevant branch is at least twofold degenerate.

We next try to understand why and how those phonon branches with labels E_2 and B_1 soften at the specific wave vectors. The relevant periods are incommensurate but are not given externally, so there should be purely internal reasons—the topology and symmetry of the idealized structure may have something to do with it. Note also that one may still wonder whether these RUMs are really RUM or not, because we have only numerical results so far.

It is worth noting that the present structure can be seen as a periodic stacking of bilayers, each of which consists of two sublayers that are mirror images of each other. Since a phonon eigenvector can only generate a deformation that is consistent with its symmetry label, the specific label would reduce the independent degrees of freedom in a single sublayer. In addition, if the phonon mode is RUM, the deformation must keep all the intertetrahedral connections without splitting. This *connectivity constraint* can further reduce the degrees of freedom within a single sublayer. For the symmetry label B_1, the independent degrees of freedom within a single sublayer are reduced to those of the displacements of two tetrahedral units out of twelve in the layer. It is readily seen that the connectivity constraint combined with the symmetry requirement prohibits translation along the *ab* plane and rotation about the *c* axis of each tetrahedral unit. Therefore, the remaining degrees of freedom are z (the translation along the c axis), θ and ϕ (the remaining degrees of freedom for rotations). The relevant coordinate axes, which are taken to be proper to each tetrahedron, are given in Figure 12. Note that the connectivity constraints at the

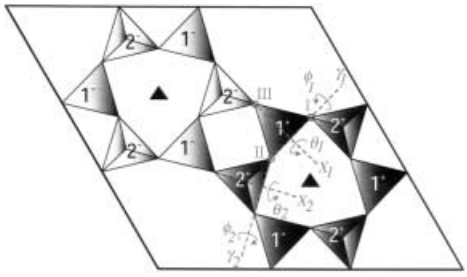

Figure 12. Within a single layer, there are only two tetrahedral units that are independent with respect to the symmetry of the irreducible representation B_1. Units with the same number and sign are distorted in exactly the same manner, while those with the same number but different signs have displacement vectors that are of equal size but opposite sign. For convenience, we chose a proper coordinate system for each tetrahedron; the axes of translation z are taken to be opposite for the units 1 and 2, while two rotational axes X and Y are given in the figure.

linkages I, II, and III impose further restrictions: $-z_1 + \theta_1 = z_2 - \theta_2$, $z_2 + \theta_2 = -z_1 - \theta_1$, and $z_1 + \sqrt{3}\phi_1 = z_2 + \sqrt{3}\phi_2$. Thus, we can conclude that there are only three independent degrees of freedom in each sublayer for RUM with this symmetry label. To represent the independent degrees of freedom, we employ the following three variables: $a = z_1 = -z_2$, $b = -z_1 - \sqrt{3}\phi_1 = -z_2 - \sqrt{3}\phi_2$, and $c = \theta_1 = -\theta_2$.

Now we consider the connectivity constraints between two successive sublayers, given by $z_2^{(-)} + \phi_2^{(-)}/\sqrt{3} = -z_1^{(+)} - \phi_1^{(+)}/\sqrt{3}$, $\theta_2^{(-)} = \theta_1^{(+)}$, and $\phi_2^{(-)} = \phi_1^{(+)}$. By using the independent variables a, b, and c defined above, these constraints can be

  0947-6539/02/0819-4554 $ 20.00+.50/0 *Chem. Eur. J.* **2002**, *8*, No. 19

rewritten as $a^{(-)} = (a^{(+)} - 2b^{(+)})/3$, $b^{(-)} = (4a^{(+)} + b^{(+)})/3$, and $c^{(-)} = -c^{(+)}$. It is convenient to write these equations as a single formula:

$$\begin{pmatrix} a^{(-)} \\ b^{(-)} \\ c^{(-)} \end{pmatrix} = T_{sub} \begin{pmatrix} a^{(+)} \\ b^{(+)} \\ c^{(+)} \end{pmatrix}, \quad T_{sub} = \begin{pmatrix} 1/3 & -2/3 & 0 \\ 4/3 & 1/3 & 0 \\ 0 & 0 & -1 \end{pmatrix},$$

in which T_{sub} is a unimodular matrix. This equation means that the displacements in a sublayer (+) determine those in a neighboring sublayer (−). If we successively multiply the matrix T_{sub}, the displacements in an arbitrary sublayer can be obtained. Note that the displacements in identical sublayers of successive bilayers are related by:

$$\begin{pmatrix} a' \\ b' \\ c' \end{pmatrix} = T \begin{pmatrix} a \\ b \\ c \end{pmatrix}, \quad T = \begin{pmatrix} -7/9 & -4/9 & 0 \\ 8/9 & -7/9 & 0 \\ 0 & 0 & 1 \end{pmatrix},$$

in which $T = T_{\mathrm{sub}}^2$ is the unimodular *transfer matrix*. The eigenvalues of the transfer matrix are read as the phase factor $e^{2\pi i\alpha}$, with α being the wave vectors for the relevant RUM, and the eigenvectors being alternative forms of the eigenvectors of the RUMs. The eigenvalues are 1 and $(-7 \pm 4\sqrt{2}i)/9$, hence the wave vectors are given by $\alpha = 0$ and $\pm(1/2\pi)\arccos(-7/9)$; the last two values are in good agreement with the ± 0.392 that was numerically obtained. It is also evident from the form of T that the degree of freedom c (equivalently θ) are independent of a and b (equivalently, z and ϕ). Therefore, the eigenvectors for $\alpha = \pm(1/2\pi)\arccos(-7/9)$ do not involve the rotation θ around the X axis; namely, the only possible rotation of each unit is around the edges that surround a threefold axes. This situation is seen in Figure 13a, in which a numerically obtained eigenvector is used to generate a deformation of a single sublayer.

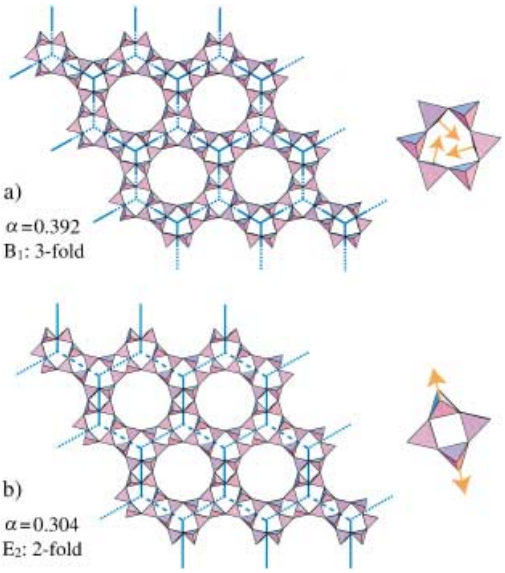

Figure 13. The deformations of a single layer corresponding to the RUMs near $\alpha = 0.392$ (a) and 0.304 (b) are shown. For each case, every single layer deforms with the same symmetry but the phase depends on the spatial position.

We have implemented a similar analysis for the case of RUMs near $\alpha = 0.304$ with the symmetry label E_2. It can be shown that the number of the degrees of freedom in a single sublayer is 9 in this case; this leads to a 9×9 transfer matrix. There are four eigenvalues which are not identical to 1, and the relevant wave vectors are exactly given by $\alpha = \pm(1/2\pi)\arccos(-1/3)$ in good agreement with ± 0.304. Again, we can show that the two allowed rotations of each tetrahedron are independent of each other, and that only one of them is relevant to this RUM. Namely, there is only rotation around the four edges that surround the twofold axes as depicted in Figure 13b.

The structural modulation is interpreted as a result of phonon condensation into one or several of the RUMs along the Δ line. For both of the incommensurate RUMs described above, each tetrahedron rotates about an axis that is parallel to the *ab* plane, thus causing the units to tilt with respect to the c axis. This makes the Si-O-Si angle decrease from the initial value of 180°. The amount to which it decreases depends on the phase of the modulation, so it depends on the spatial position. Well below the transition temperature, however, as thermal fluctuation is overcome by the energy effect, all the Si-O-Si angles tend to be around 140–150°. Therefore, slowly varying modulation is replaced by a discontinuous pleat pattern as shown in Figure 5. In our analysis, the incommensurate RUM with B_1 symmetry is most likely to be responsible. Meanwhile, some of the RUMs at the Γ point must be responsible for the symmetry breaking associated with the vanishing of *c* glides.

As a final remark, it is difficult to identify the relevant RUMs for the actual deformation just from the RUM context, since it provides all possible soft deformations of the ideal predeformed structure. A more realistic model could handle this point if it took nonlinearity effects into account. Still, our theory provides an insight into the origin of the modulation in SSZ-24 in a comprehensive way.

Acknowledgements

A part of this study was supported by the CREST project, JST(OT). Z.L. and N.F. thank the JST for support. For the numerical analyses of our RUM model, we used the Fortran codes, CRUSH, IDEALISER, and GROUP, which are freely distributed on the web by the authors of Ref. [9].

[1] J. M. Bennet, J. P. Cohen, E. M. Flangen, J. J. Pluth, J. V. Smith, *ACS Symp. Ser.* **1983**, *218*, 109.
[2] S. Qiu, W. Pang, H. Kessler, J. L. Guth, *Zeolites* **1989**, *9*, 440.
[3] J. W. Richardson, J. J. Pluth, J. V. Smith, *Acta Crystallogr. Sect. C* **1987**, *43*, 1469.
[4] R. Bialek, W. M. Meier, M. Davis, M. J. Annen, *Zeolites* **1991**, *11*, 438.
[5] T. Ikeda, K. Miyazawa, F. Izumi, Q. Huang, A. Santoro, *J. Phys. Chem. Solids* **1999**, *60*, 1531.
[6] A. Rabdel Ruiz-Salvador, G. Sastre, D. W. Lewis, C. Richard, A. Catlow, *J. Mater. Chem.* **1996**, *6*, 1837.
[7] A. J. Mora, A. N. Fitch, M. Cole, R. Goyal, R. H. Jones, H. Jobic, S. W. Carr, *J. Mater. Chem.* **1996**, *6*, 1831.
[8] A. P. Giddy, M. T. Dove, G. S. Pawley, V. Heine, *Acta Crystallogr. A* **1993**, 49, 697.
[9] K. D. Hammonds, M. T. Dove, A. P. Giddy, V. Heine, *Am. Mineral.* **1994**, *79*, 1207.

  0947-6539/02/0819-4555 $ 20.00+.50/0

[10] K. D. Hammonds, V. Heine, M. T. Dove, *J. Phys. Chem. B* **1998**, *102*, 1759.
[11] K. D. Hammonds, F. Deng, V. Heine, M. T. Dove, *Phys. Rev. Lett.* **1997**, *78*, 3701.
[12] Y. Nakagawa, US patent 5,271,922, **1993**.
[13] M. A. Camblor, M. J. Díaz-Cabañas, J. Pérez-Pariente, S. J. Teat, W. Clegg, I. J. Shannon, P. Lightfoot, P. A. Wright, R. E. Morris, *Angew. Chem.* **1998**, *110*, 2234; *Angew. Chem. Int. Ed.* **1998**, *37*, 2122.
[14] J. L. Guth, R. Wey, *Bull. Soc. Fr. Minéral. Cristallogr.* **1969**, *92*, 105.

Received: February 5, 2002
Revised: June 14, 2002 [F3854]

0947-6539/02/0819-4556 $ 20.00+.50/0